

Stress and Vibration Analysis of Turbopump Inducer Blades by Finite Elements

H. J. BARTEN* AND J. A. SCHEURENBRAND†

Pratt & Whitney Aircraft, Florida Research and Development Center, West Palm Beach, Fla.

AND

D. D. SCHEER‡

NASA Lewis Research Center, Cleveland, Ohio

This paper discusses the formulation of stress and vibration analysis programs for use on rocket engine turbopump inducer blades. The analytical model is based on the matrix displacement method using discrete, flat triangular elements to define the blade surface. The stress program calculates stress magnitude and distribution caused by pressure loading and centrifugal forces. The vibration program calculates natural frequencies and distribution of relative displacements and stresses at resonance for a nonrotating inducer blade. The capabilities of the computer programs are demonstrated, and experimental static and operational test data indicate that the programs are capable of predicting frequencies, points of maximum stress, and maximum stress levels.

Nomenclature

$\{F_c\}_{NT}$	= system nodal centrifugal force matrix
$\{F_p\}_{NT}$	= system nodal pressure force matrix
F_x, F_y, F_z	= nodal forces in common system
$[I]$	= unit matrix
$[K_B]^*$	= reduced system bending stiffness matrix
$[K]_T$	= system stiffness matrix
$[M_B]^*$	= reduced system bending mass matrix
M_x, M_y, M_z	= nodal moments in common system
NPSH	= net positive suction head
R_G	= offset cylinder radius
R^*	= distance along generator from offset cylinder
R	= projection of R^* on x, y plane
u, v, w	= inducer surface displacements in common system
x, y, z	= inducer surface coordinates in common system
x_n, y_n, z_n	= inducer surface coordinates in quasi-normal system
$\{\delta\}_{NT}$	= system nodal displacement matrix
θ	= wrap angle
$\theta_x, \theta_y, \theta_z$	= inducer surface rotations in common system
λ	= generator lean angle
σ_{eff}	= effective stress
σ_x, σ_y	= principal stresses
ϕ	= flow coefficient
ω	= natural frequency

Subscripts

1, 2, 3	= values at nodes
H	= hub,
T	= tip

Superscript

(-)	= local coordinates
-----	---------------------

Introduction

OVER-ALL vehicle weight advantages associated with liquid-rocket pump operation at high-speed and low-inlet pressure have been achieved by using high suction specific speed inducers as the initial pumping element in propellant feed systems. Methods have been developed for predicting inducer suction capability and head rise accurately. Structural design, however, has not received systematic attention, and it has been necessary for designers to make conservative allowance for the structural prediction uncertainties. As a result, the hydrodynamic design was frequently compromised.

To provide a structurally adequate inducer and at the same time maintain hydrodynamically favorable blade thickness, the designer must be able to predict centrifugal load, pressure load, and resultant stresses. Additionally, a knowledge of inducer blade natural frequencies is required, so that blade resonance with known forcing stimuli can be avoided. Problems identified in these areas included pressure load prediction as well as stress and natural frequency prediction. The pressure distribution over the entire blade surface was usually estimated by two separate approaches. Pressure load on the blade leading edge was usually predicted by applying the free-streamline-wake model of Stripling and Acosta.¹ In the channel region, a two-dimensional axisymmetric model for no loss, noncavitating flow was used. Steady-state stress was predicted by dividing the inducer into pie-shaped segments and applying simple plate or beam theory or, in some of the later designs, by modeling the blade as a variable thickness, flat plate and employing finite element techniques. Blade natural frequencies were usually determined experimentally after an inducer had been fabricated.

Effort was initiated by the NASA Lewis Research Center to obtain analytical models which could predict inducer blade steady-state pressure loading under cavitating and noncavitating conditions, steady state stress magnitude and distribution due to centrifugal and hydrodynamic loading, and blade natural frequencies and relative stresses at resonance. The results of the effort accomplished in the area of hydrodynamic load prediction are given in Ref. 2.

This paper discusses the formulation and capabilities of these computer programs. The inducer surface is replaced

Presented as Paper 70-680 at the AIAA 6th Propulsion Joint Specialist Conference; San Diego, Calif. June 15-19, 1970; submitted July 16, 1970; revision received February 4, 1971. This work was carried out at the Florida Research and Development Center of Pratt & Whitney Aircraft for the NASA Lewis Research Center, Chemical Rockets Division, under Contract NAS3-11216. All support is gratefully acknowledged.

* Assistant Design Project Engineer. Member AIAA.

† Digital Computer Engineer.

‡ Project Manager. Member AIAA.

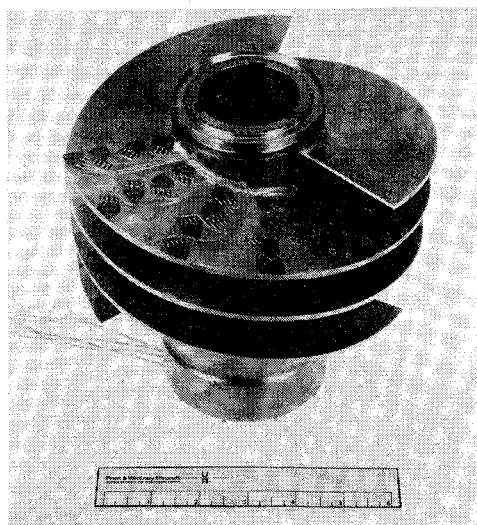


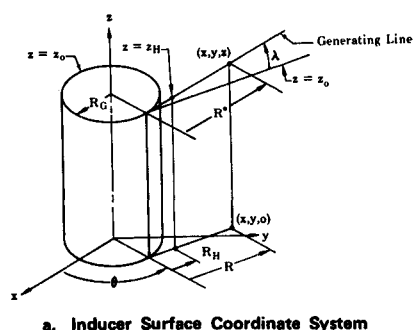
Fig. 1 Typical AMS 4928 inducer strain gaged for test.

by discrete, flat triangular elements. Provisions are incorporated for handling uniformly tapered blades. The static program predicts stresses and displacements due to variable blade pressure and centrifugal loads. The vibration program predicts natural frequencies, mode shapes, and relative bending stresses due to free vibrations. Test cases on simple geometric shapes with known solutions were followed by correlation of predicted results with test data.

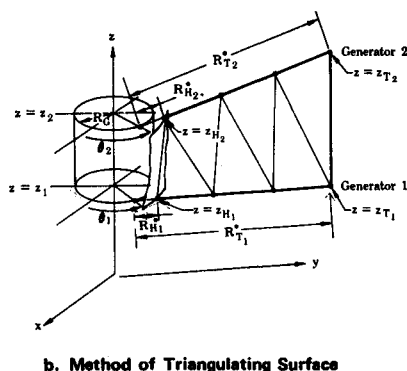
Development of Programs

Inducer Surface Coordinates

A typical inducer is shown in Fig. 1. From the beginning it was evident that an efficient method of determining the coordinates of the middle surface of such inducers would be



a. Inducer Surface Coordinate System



b. Method of Triangulating Surface

Fig. 2 Inducer surface coordinate system and method of triangulating surface.

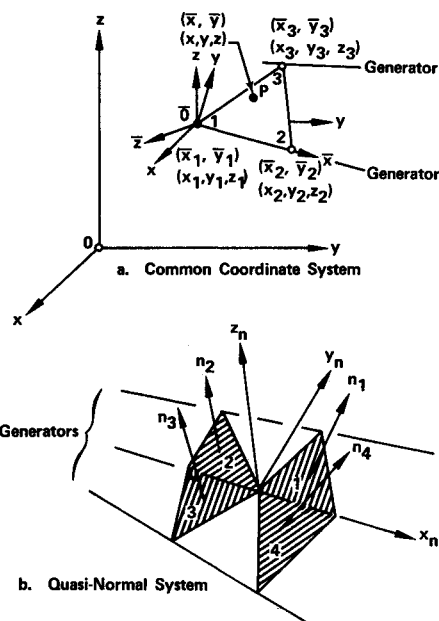


Fig. 3 Coordinate systems.

necessary, whether direct mathematical or approximate analyses were to be used. From an engineering and computer oriented standpoint, the inducer surface is best defined by its natural helicoidal coordinates, which are defined by points on skewed generating lines whose positions in space are specified. With the surface defined in this manner, the (x, y, z) coordinates of points on a generator line will always be in a linear relation which can be used to advantage by the analyst and the computer. Parameters that define the position of the skewed generating line as shown in Fig. 2a are offset radius, R_G ; hub radius z distance, z_H ; hub radius tangent distance, R_H ; generator lean angle λ ; and wrap angle, θ . The relations for the (x, y, z) coordinates of a point on a generator expressed in a right-handed rectangular coordinate system are then: $x = R_G \cos \theta - R \sin \theta$; $y = R_G \sin \theta + R \cos \theta$; $z = z_H + (R - R_H) \tan \lambda$; where R is the projection of the running distance R^* on the $(x, y, 0)$ plane. The generator line is skewed or offset, because the intersection of a surface generated in this manner with a plane through the z axis and at a fixed wrap angle is curved. This provides additional flexibility in describing not only typical inducer surfaces, but also impellers, curved blades, marine propellers, etc. This tangential coordinate system is advantageous to the analyst and designer, because it not only provides the parameters necessary for machining, but it also ties the stress program directly to the hydrodynamic load program which provides blade loading for predicting stresses in inducer blades.²

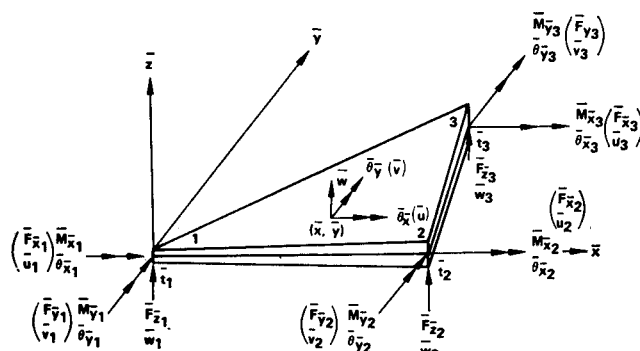


Fig. 4 Local nodal displacement and force systems.

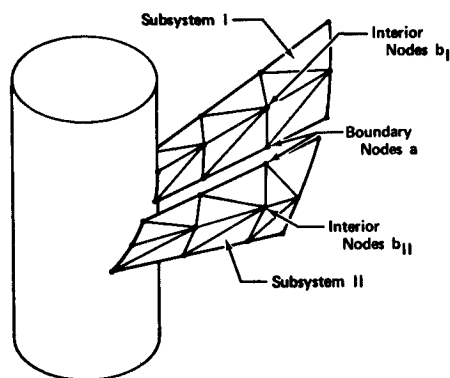


Fig. 5 Division of system into subsystems.

Approximation of Surface by Flat Triangular Elements

An extensive literature survey indicated that theoretical solutions for determining the stress and vibration characteristics of inducer type shells were nonexistent. This survey also indicated that the finite element matrix displacement method was the most powerful method available for such analyses.³⁻⁶ In this method the surface is replaced by contiguous polygonal elastic elements of finite sizes which are joined at their vertices or nodes. Nodal displacements are then determined by using the combined stiffness of the elements under the action of statically equivalent nodal forces. Because of the twisted nature of the inducer surface, the nodes of any polygon of more than three sides would not lie in a plane, and a three-dimensional element stiffness matrix would be required. For this reason the inducer surface is approximated by contiguous flat triangular elements which require only two-dimensional element stiffness matrices, and for which the change in direction of their normals is an indication of geometric curvature. This is accomplished in the computer program by first dividing the distance along generators between the hub and the tip into equally spaced nodes and then joining these nodes with the nodes on adjacent generators as shown in Fig. 2b. Thus, the additional parameters necessary for triangulation are the tip radius R_T^* and the nodal spacing. Triangular elements are assembled in the same manner for the stress and vibration program.

Local, Common, and Quasi-Normal Coordinate Systems

A local, right-handed, two-dimensional (\bar{x}, \bar{y}) coordinate system as shown in Fig. 3a was adopted for the triangular elements. The base of each element contains node 1 and node 2 and the \bar{x} axis. When the elements are assembled to approximate the surface in the common or global (x, y, z) system, the origin \bar{O} and \bar{x} axis lie on one generator, and node 3 lies on the adjacent generator. After assembly the direc-

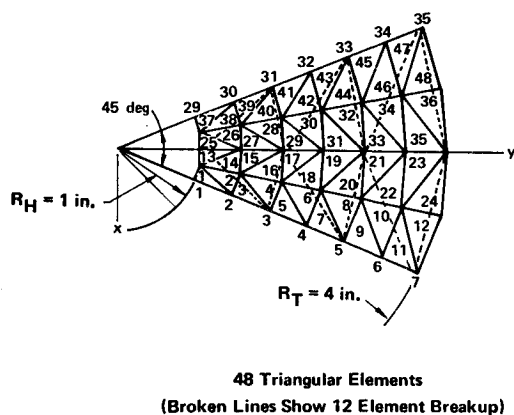


Fig. 6 Breakup of 45-degree sector. (broken lines show 12 element breakup)

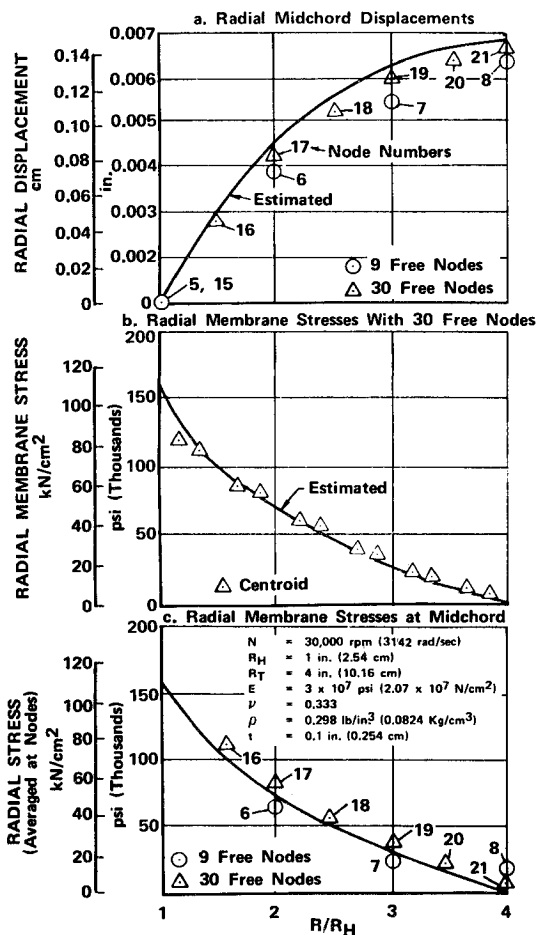


Fig. 7 Radial displacements and membrane stresses in rotating 45° sector.

tion cosine matrices $[R_i]$ are determined. These matrices relate the directions of the local (\bar{x}, \bar{y}) axes of each element to the directions of the common (x, y, z) axes.

For the vibration program a quasi-normal right-handed coordinate system is used. This system is shown in Fig. 3b. In this system the x_n axis lies along a generator and the z_n axis has a direction which is the mean direction of the surface normals, n , of the triangular elements whose bases lie on a common generator as shown. The y_n axis is then perpendicular to the x_n and z_n axes in a right-handed sense direction. This system was adopted for the vibration program, because the predominant amplitudes were assumed to be in a direction normal to the inducer surface.

Provisions are also made for a transition of the breakup in going from one generator to the next. This allows for fine breakups in highly loaded regions where increased accuracy is desired and coarse breakups in noncritical regions. Such a transition is also required for describing swept leading edge geometry.

Implementation of Matrix Displacement Method

The approximation of the surface by finite elements connected only at the nodes means that loads can be transmitted from element to element only through the nodes, thus requiring the replacement of distributed boundary forces by statically equivalent concentrated nodal forces. In order to use the matrix displacement method, displacement functions must be selected that approximate the displacement modes of points in the element. A membrane displacement function and a bending displacement function are used for

§ Typical applications of this technique are shown in Figs. 12 and 16.

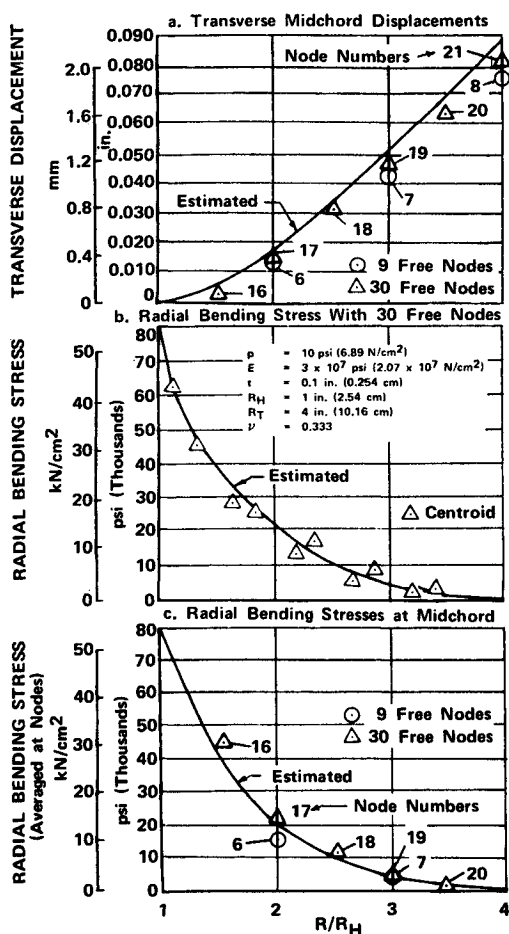


Fig. 8 Midchord displacement and radial bending stresses in uniformly loaded 45° cantilevered sector.

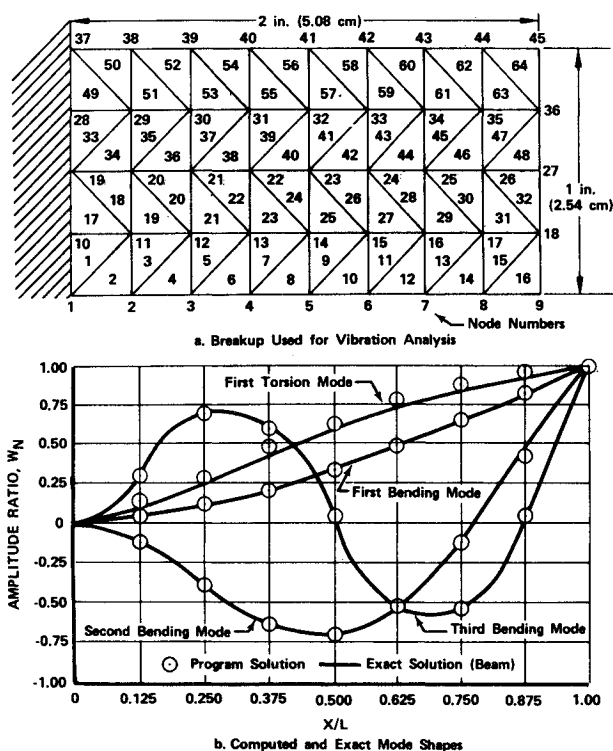


Fig. 9 Comparison of mode shapes of 1 in. \times 2 in. rectangular plate.

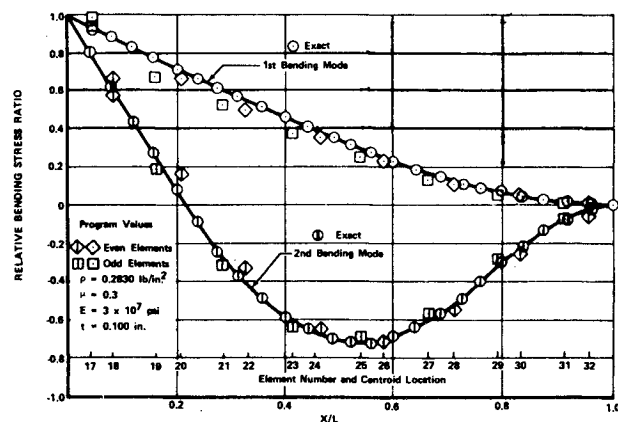


Fig. 10 Relative vibratory bending stresses in a cantilever beam (2 \times 1). (See Fig. 9a)

the inducer programs. The membrane displacement function is linear in \bar{x} and \bar{y} and yields a constant strain triangle with two degrees of freedom at each node. The bending displacement function is a cubic polynomial in \bar{x} and \bar{y} with nine coefficients and yields a triangle with three degrees of freedom at each node. This latter function does not provide continuity in slope at adjoining edges, resulting in incompatible triangles and a possible reduction in accuracy. Compatible triangles can be obtained by techniques discussed in Ref. 6 but were not used in this program because of increased storage. The local nodal displacement and nodal force system used for the membrane and bending modes are shown in Fig. 4.

The stress and vibration programs are discussed separately below because of the dissimilarity of the coordinate systems used.

Stress program

The selected displacement functions are used to calculate 18×18 membrane and bending stiffness matrices and 18×1 pressure and centrifugal force matrices in the local coordinate system of each triangular element. These matrices involve an integration by Gaussian quadrature because of the provision for variable blade thickness. They are then transformed to the common system using the appropriate 18×18 direction cosine matrices. The elements of these matrices are then collected at the n free nodes, and the summation of nodal forces and equating of nodal displacements yields the $6n \times 6n$ system matrix relation

$$[K]_T \{\delta\}_{NT} - \{F_p\}_{NT} - \{F_c\}_{NT} = \{O\}$$

where $[K]_T$ = system stiffness matrix; $\{\delta\}_{NT}$ = system nodal displacement matrix; $\{F_p\}_{NT}$ = system nodal pressure force matrix; $\{F_c\}_{NT}$ = system nodal centrifugal force matrix.

This set of simultaneous equations is then solved for the nodal displacement matrix $\{\delta\}_{NT}$ by the Gauss elimination method, and nodal displacements in the local system are obtained by applying the inverse of the direction cosine matrix. Local stresses, based on the assumed displacement functions, are then calculated. The program prints out radial stresses, tangential stresses, shear stresses, principal stresses, effective stresses, and nodal displacements for each element in its local system and the displacements of the n free nodes in the common system. Membrane and bending stresses are also combined for design purposes and segregated for examination of coupling effects. The bending stresses for each element are calculated at their centroid, and linear coefficients are provided for calculating the bending stress at any point in an element. The effective stress, based on the energy of distortion theory in terms of the principal

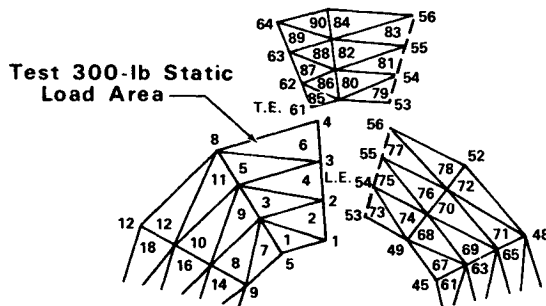


Fig. 11 Partial layout of 90-element breakup of inducer blade.

stresses σ_x and σ_y is

$$\sigma_{\text{eff}} = (\sigma_x^2 + \sigma_y^2 - \sigma_x \sigma_y)^{1/2}$$

The computer capacity limits the number of free nodes to 150, which is equivalent to 900 simultaneous equations. Execution time for handling such a system is prohibitive. For this reason an option is provided for subsystem analysis. A representative division of the system into subsystems is shown in Fig. 5. This is a conventional technique in which the analysis is accomplished by partitioning the nodal force-displacement matrix relation to separate boundary and interior nodes. The program allows a maximum of 10 subsystems and a total of 200 nodes, including hub nodes, with minor restrictions on the number of subsystem nodes.

An option for providing symmetrical back-to-back breakups, as shown in Fig. 6, was provided after it was found that antisymmetrical breakups did not yield symmetrical solutions when symmetrical loading was used. This type of breakup is used predominantly; also, an option provides anti-symmetrical breakups which will occur for transition geometries and swept leading edge geometries.

Vibration program

Due to the limitations of the eigenvalue subroutine, a maximum of 50 free nodes is permitted, thus possibly necessitating a different breakup than the stress program. The selected displacement functions are used to calculate 18×18 mass and stiffness matrices in the local coordinate system of each triangular element. These matrices are transformed to the quasi-normal system using the appropriate 18×18 direction cosine matrices. The elements of these matrices are then collected at the n free nodes in the same manner as used in the stress program yielding the $6n \times 6n$ system matrix. By assuming that twisting displacements about the normal to the surface and membrane displacements are negligible, and that the predominate motion is in the normal direction, this system is reduced to one of $3n$ degrees-of-freedom. The resulting system is then partitioned to separate the $n \times 1$ nodal normal displacement system matrix from the $2n \times 1$ nodal rotational displacement system matrix. The $3n$ degree-of-freedom system is then further reduced to an n degree-of-freedom system by a matrix condensation technique recommended by Guyan.³ This admits the $n \times n$ frequency equation:

$$[-\omega^2[I] + [M_B]^*^{-1}[K_B]^*] = 0$$

where $[M_B]^*$ and $[K_B]^*$ are reduced mass and stiffness system matrices. After the frequencies are determined by the program, the displacements are determined by normalizing with the maximum nodal displacement. Local nodal displacements for each element are determined by applying the inverse of the normal direction cosine matrix. The local nodal displacements are then used to calculate the effective bending stresses at the centroid of each element. These stresses are normalized with the maximum stress and are

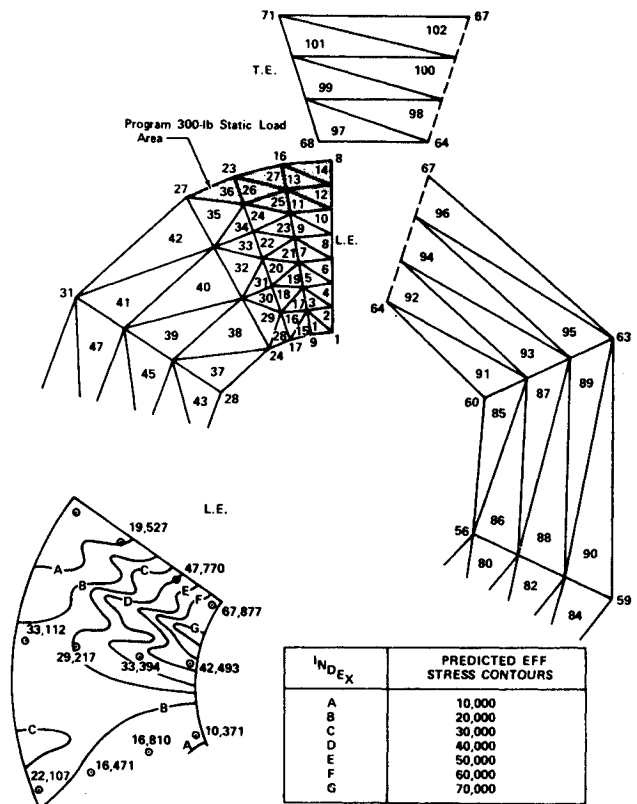


Fig. 12 102-element breakup for static load stress analysis and comparison of measured and predicted effective stresses.

printed out as relative vibratory stresses, along with nodal amplitudes and frequencies for each mode.

Discussion of Typical Results of Analyses

Test cases were first run on flat surfaces by using a special matrix. This was done to obtain two-dimensional solutions that could be compared with known two-dimensional solutions. Flat plate geometries cannot be run with the existing three-dimensional program because the system matrix becomes singular. For this reason all of the test cases were re-run with the final program by programming the surface so that it was slightly warped out of plane. The results of these re-runs agreed just as closely to the theoretical values for flat plates as did the first flat plate runs. The same technique was used for the vibration program test cases on flat plates.

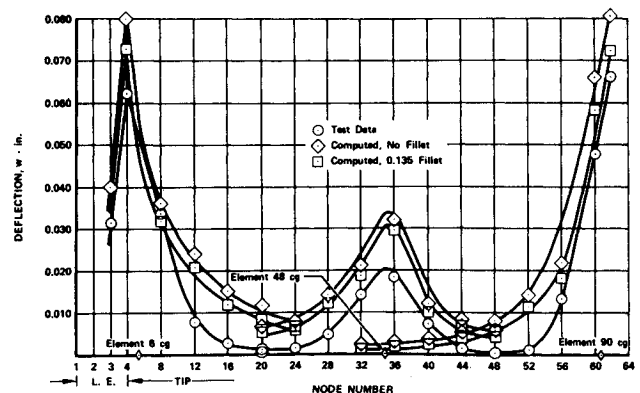


Fig. 13 Deflection of inducer blade under static load (See Fig. 11)

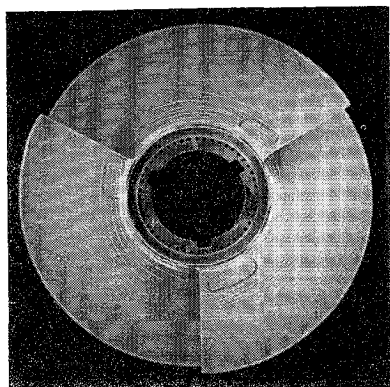


Fig. 14 Umbrella mode stress coat patterns on test inducer. (Enclosures indicate areas of high stress)

Stress Program

Test cases were run on 45° flat sectors with 9 and 30 (Fig. 6) free nodes under uniform transverse load and centrifugal loading. There was a decided improvement in predicting radial displacements for the centrifugal load case in going from 9 to 30 nodes as is shown in Fig. 7a. Radial membrane stresses on interior triangular elements just about straddled the estimated stress curve when they were plotted at the centroid of the appropriate triangle, as shown in Fig. 7b. Approximate stresses and displacements were estimated by direct integration assuming that the radial pull is independent of polar angle. Averaging the stresses at each node by averaging the stresses in the triangles immediately surrounding a node also agreed fairly well with the estimated curve, as shown in Fig. 7c.

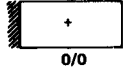
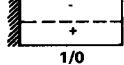
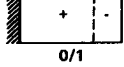
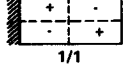
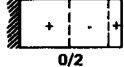
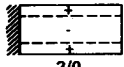
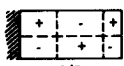
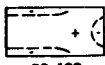
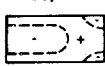
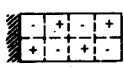
The predictions of displacements under bending load also were improved in going from 9 to 30 nodes, as shown in Fig. 8a. Radial bending stresses on interior triangular elements also straddled the estimated curve, as shown in Fig. 8b. These stresses were also averaged at the center nodes and are presented in Fig. 8c. Stresses were obtained from the moment distribution on a cantilever beam of linearly varying width, and displacements were approximated by the moment-area method.

Vibration Program

Rectangular plate

A test case on a 1×2 in. (2.5×5.1 cm) rectangular plate with 40 free nodes yielded the results shown in Fig. 9 and Table 1. The predicted first four mode shapes agree closely with the exact mode shapes as shown in Fig. 9. The predicted frequencies and mode orders, however, do not agree

Table 1 Comparison of exact and computed modes and natural frequencies of $1 \times 2 \times 0.1$ in. thick cantilevered rectangular steel plates

Mode ^a	Exact (Reference 5)	Frequencies, Hz	
		Existing Program	Present Program
 0/0	846	844	720
 1/0	3,638	3,584	4,942
 0/1	5,266	5,301	4,513
 1/1	11,870	11,802	14,648
 0/2		15,185	12,532
 2/0		23,011	21,563
 1/2		23,340	25,165
 0/3		29,469	24,459
 2/1		31,190	35,039
 1/3		38,331	38,175

^aFirst number is number of x nodes and second number is number of y nodes

with exact values,⁵ whereas there is close agreement from an existing flat plate program using rectangular elements as shown in Table 1. It was suspected that the combination of "incompatible" triangular elements and the slender 2:1 length/width ratio rectangle caused the discrepancy in frequencies and mode orders. Analysis of a wide 1:2 length/width ratio rectangle resulted in much closer agreement of frequencies and agreement in mode orders. Since an inducer is essentially a wide beam with a small length/width ratio, it was concluded that the vibration program should be applicable to inducers.

Figure 10 shows relative centroidal vibratory bending stresses for the same 1×2 in. rectangular plate as compared to the theoretical values for a cantilevered beam of the same shape. The agreement is good except near the clamped edge.

Typical inducer

A test case was conducted for an inducer with a 6° blade angle and a 438° wrap angle. Results compared with test data as shown in Table 2. The results were in fairly good agreement, at least through the fifth mode.

Experimental Verification

The capabilities of the computer programs were demonstrated by experimental static, dynamic, and operational tests on a set of identical inducers, which were designed and fabricated specifically for this purpose. The design and testing of the inducer is discussed in detail in Ref. 7. Table 3 compares predicted and measured maximum stresses as obtained from these tests.

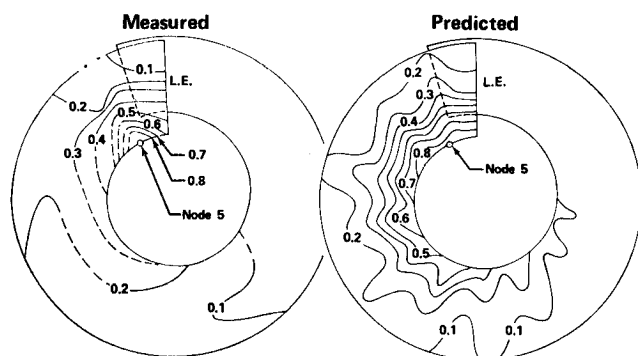

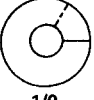
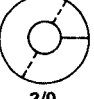
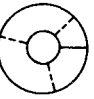
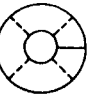
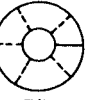
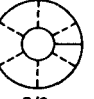


Fig. 15 Relative first-mode effective stress contours.

Table 2 Mode shapes and comparison of natural frequencies of 6° (0.105-rad) inducer

Mode ^a	Frequency, cps	
	Test Data	Calculated (Present Program)
	441	483
0/0 (Umbrella)		
	575	540
1/0		
	---	606
2/0		
	---	709
3/0		
	831	840
4/0		
	---	994
5/0		
	957	1170
6/0		

^a First number is number of radial nodes and second number is number of circumferential nodes.

One inducer was instrumented with rosette strain gages and the other with blade surface pressure taps. The strain-gaged inducer is shown in Fig. 1. Gages were located at the nodes of the 90-element breakup shown in Fig. 11. Strain data from these gages were used to calculate the effective stress at each node for comparison with predicted values. Pertinent details of these tests are in Table 3.

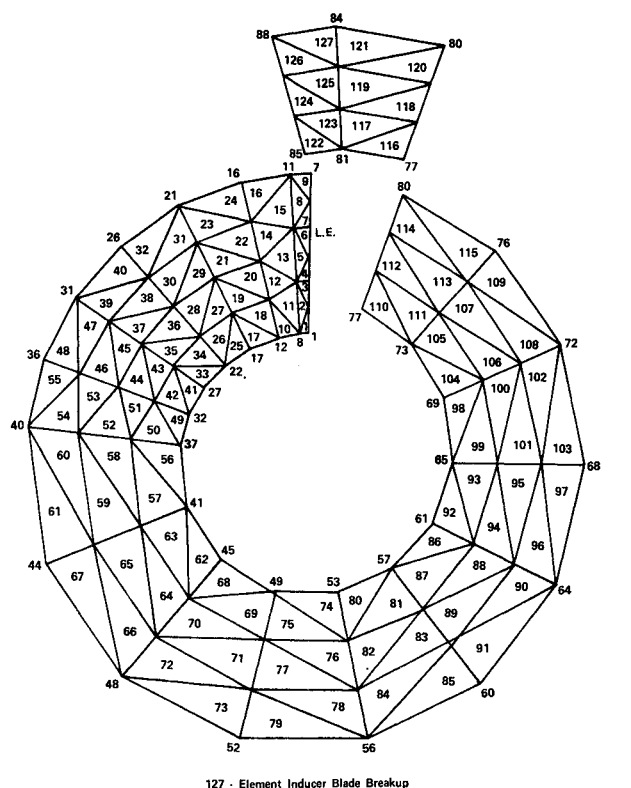
Static Stresses

Static tests were conducted on the inducer by applying a concentrated load of 300 pounds separately at the leading

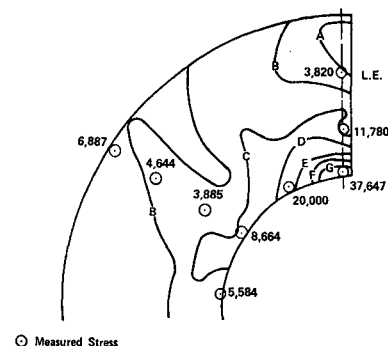
Table 3 Comparison of values of maximum stress on test inducer

Type ^a Test	φ	%N	NPSH	Max Stress (Thousands)			
				Predicted lb/in ²	N/cm ²	Test lb/in ²	N/cm ²
S (LE)				70	48	68	47
S (M)				30	21	29	20
S (TE)				80	55	83.5	58
O (NC)	0.090	80	106	22.5	15.5	24	17
O (NC)	0.096	100	106	36.5	25.2	38	26
O (NC)	0.090	100	106	39	26.9	41	28
O (NC)	0.084	100	106	45.5	31.3	46	32
O (C)	0.089	100	50	34	23.4	25	17

^a S = Static Load
LE = Leading Edge Tip
M = Midchord Tip
TE = Trailing Edge Tip
O = Operational
C = Cavitating
NC = Non-Cavitating
100% N = 4900 rpm



INDEX	PREDICTED EFF STRESS CONTOURS
A	2,500
B	5,000
C	10,000
D	15,000
E	20,000
F	25,000
G	30,000
H	35,000

**Fig. 16 127-element breakup for hydrodynamic load stress analysis and comparison of predicted and measured stresses.**

edge tip, midchord tip, and trailing edge tip. A comparison of test results and predicted results for the leading edge test is shown in Fig. 12. It should be noted that the predicted values are based on a 102-element breakup which is coarse at the trailing edge where the stresses are low and fine at the leading edge where the stresses are higher and more accuracy is desired. Agreement is generally good, particularly at the maximum stress point near the leading edge hub.

Static Deflections

Deflections due to a 200-lb load applied separately at the leading edge tip, midchord tip, and the trailing edge tip were also measured during static tests. Fig. 13 shows the measured and predicted deflections. Large deflections show better agreement than small deflections, and the effect of using the actual hub diameter and the effective hub diameter which is located at the blade-fillet tangency point is shown.

Relative Vibratory Stresses and Natural Frequencies

Vibratory tests on a stress-coated inducer indicated high stresses at the L.E. hub for the first few modes. A typical stress-coat patterns for the first mode is shown in Fig. 14.

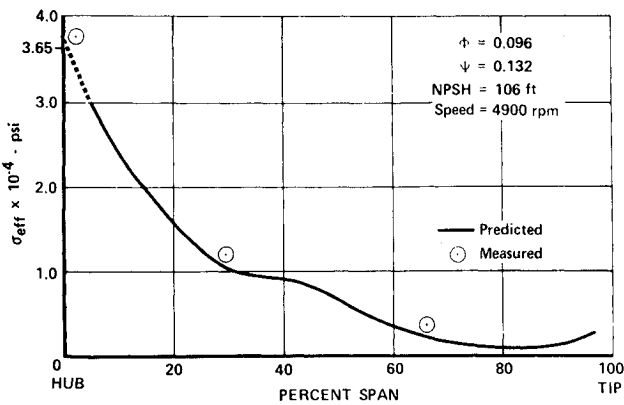


Fig. 17 Distribution of stress with radius at leading edge.

Strain gage data from vibratory tests were used to calculate relative effective stress contours for comparison with predicted contours. The comparison of results for the first mode are shown in Fig. 15. The point of maximum stress at the leading edge hub is predicted, and the agreement is generally good except for "wiggles" in the predicted contours.

Measured natural frequencies and tip node positions are compared with predicted values in Table 4. The agreement of frequencies at lower modes is good, with the error increasing as the higher modes are excited. Tip node positions do not agree as closely as is desired, although they show the proper trend.

Operational Tests

Operation tests were performed on the inducer in a rig. Strains and pressures were measured on separate runs with the inducer operating at the same conditions. Measured and predicted hydrodynamic loads on the inducer surface were input into the stress program. A 127-element breakup as shown in Fig. 16 was used for stress analysis because of the high gradient in leading edge hydrodynamic loading. Pre-

dicted stress contours and measured stresses for a typical run are shown in Fig. 16. The leading edge stresses at the hub were obtained by extrapolation of predicted data as shown on the curve in Fig. 17. This curve corresponds to the dashed line in Fig. 16 and falls very close to the measured stresses as shown. Fig. 16 indicates that the predicted position of maximum stress agrees with that shown by test, and the predicted maximum stress of 36,500 psi is in good agreement with the measured maximum stress of 37,600 psi.

Summary

The capability of computer programs developed for the prediction of structural and dynamic characteristics of inducers has been demonstrated by comparing predicted results with the results of other theoretical analysis and with experimental data. In general, predicted values show good agreement with exact and measured results. There are still a number of areas which can probably be improved by modification of the programs. Discrepancies which occur in the predictions always seem to point to the necessity of using so-called "compatible" triangles which are not used in these programs. Stiffness matrices for such triangles are derived so that the normal slope between common edges of triangles are equal. This technique guarantees that the solution will approach an asymptotic value monotonically and will not oscillate as the element is made smaller.

It is suspected that the vibration program can be improved by not only using "compatible" triangles, but by also using a finer breakup. Since the eigenvalue program limits the breakup to only 50 free nodes, a finer breakup can be achieved only by increasing the allowable number of nodes to more than 50. This can be accomplished by using either an iteration technique, an eigenvalue subroutine which requires more computer storage, or a subsystem analysis in a manner similar to that which was used in the stress program.

It would also be advantageous to marry the two programs by solving the eigenvalue problem in the common system so that no approximations to the direction of blade motion would have to be made. The potential of these programs can be increased by providing methods to incorporate: arbitrarily varying blade thickness, prescribed boundary displacements, variable offset radius, thermal stresses, shear deformation, forced vibrations, and equal leading edge and trailing edge displacements, wrap angles and z coordinates for analysis of complete shells.

References

- ¹ Stripling, L. B. and Acosta, A. J., "Cavitation in Turbopumps, Parts 1 and 2," Papers 61-WA-112 and 61-WA-98 presented at the Winter Annual Meeting of the American Society of Mechanical Engineers, New York, Nov. 26-Dec. 1, 1961.
- ² Davis, R. E., Coons, L. L., and Scheer, D. D., "Internal Streamline Flow Analysis for Turbopump Inducers Under Cavitating and Non-Cavitating Conditions," AIAA Paper 70-629, San Diego, Calif., 1970.
- ³ Guyan, R. J., "Reduction of Stiffness and Mass Matrices," *AIAA Journal*, Vol. 3, No. 2, Feb. 1965, p. 380.
- ⁴ Zienkiewicz, O. C. and Y. K. Cheung, *The Finite Element Method in Structural and Continuum Mechanics*, 1st ed., McGraw Hill, New York, 1967.
- ⁵ Barton, M. V., "Vibration of Rectangular and Skew Cantilever Plates," *ASME Journal of Applied Mechanics*, Vol. 18, No. 2, June 1951, pp. 129-134.
- ⁶ "Matrix Methods in Structural Mechanics," *Proceedings of Wright-Patterson Air Force Base Conference*, Rept. AFFDL-TR-66-80, Oct. 1965, Wright-Patterson Air Force Base.
- ⁷ Final Report, "Study of Inducer Load and Stress," Rept. PWA FR-7304, CR 72712, Dec. 1970, NASA.

Table 4 Predicted and experimental natural frequencies of test inducer (Fig. 1)

Mode*	Predicted Frequency, Hz	Predicted Tip Node Position	Experimental Frequency, Hz	Error	Experimental Tip Node Position
0/0* (Umbrella)	1105		1067	3.5%	
1/0	1262		1245	1.3%	
2/0	1438		1408	2.1%	
3/0	1583		1522	4.0%	
4/0	1782		1640	7.4%	
5/0	2019		1740	16%	
6/0	2294		1947	18%	
7/0	2709		2158	26%	
8/0	3127		
9/0	3633		2858	27%	
10/0	4167		3284	27%	
11/0	4751		
12/0	5345		3415	24%	

*First number is number of radial nodes and second number is number of circumferential nodes.